Compressed Motion Sensing

Robert Dalitz[1], Stefania Petra[1(✉)], and Christoph Schnörr[2]

[1] MIG, Institute of Applied Mathematics, Heidelberg University, Heidelberg, Germany
robert.dalitz@iwr.uni-heidelberg.de, petra@math.uni-heidelberg.de
[2] IPA, Institute of Applied Mathematics, Heidelberg University, Heidelberg, Germany
schnoerr@math.uni-heidelberg.de

Abstract. We consider the problem of sparse signal recovery in *dynamic* sensing scenarios. Specifically, we study the recovery of a sparse *time-varying* signal from linear measurements of a *single* static sensor that are taken at two different points in time. This setup can be modelled as observing a single signal using two different sensors – a real one and a virtual one induced by signal motion, and we examine the recovery properties of the resulting combined sensor. We show that not only can the signal be uniquely recovered with overwhelming probability by linear programming, but also the correspondence of signal values (signal motion) can be established between the two points in time. In particular, we show that in our scenario the performance of an undersampling static sensor is doubled or, equivalently, that the number of sufficient measurements of a static sensor is halved.

1 Introduction

Overview, Motivation. On of the most common scenarios of compressed sensing concerns the unique recovery of a sparse vector $x \in \mathbb{R}^n$ from $m < n$ linear measurements by ℓ_1-norm minimization,

$$\min_{x \in \mathbb{R}^n} \|x\|_1 \quad \text{subject to} \quad Ax = b_x, \tag{1}$$

based on suitable conditions on the sensor matrix A [3]. In this paper, we extend this scenario in that x undergoes some unknown transformation,

$$y = T(x), \tag{2}$$

and then is observed once more by the *same* sensor: $Ay = b_y$. The corresponding extension of (1) reads

$$\min_{x,y \in \mathbb{R}^n} \left\| \begin{pmatrix} x \\ y \end{pmatrix} \right\|_1 \quad \text{subject to} \quad \begin{pmatrix} A & 0 \\ 0 & A \end{pmatrix} \begin{pmatrix} x \\ y \end{pmatrix} = \begin{pmatrix} b_x \\ b_y \end{pmatrix}. \tag{3}$$

Acknowledgments. We gratefully acknowledge support by the German Science Foundation, grant GRK 1653.

© Springer International Publishing AG 2017
F. Lauze et al. (Eds.): SSVM 2017, LNCS 10302, pp. 602–613, 2017.
DOI: 10.1007/978-3-319-58771-4_48

This formulation, however, merely doubles the number of measurements to $2m$ and the number of variables to be recovered to $2n$. Additionally, it has the weakness that the additional m linear measurements are not independent.

On the other hand, if the transformation T of (2) was *known*, then the number of variables to be recovered remains n, because the *same* vector x is observed in two different ways. Moreover, suppose the measurements (2) of the transformed vector can be approximated by $A(T)x \approx AT(x)$ in terms of a *virtual* sensor $A(T)$ (regarded as a function of T), then the number of measurements is *effectively* doubled to $2m$ and the recovery problem reads

$$\min_{x\in\mathbb{R}^n} \|x\|_1 \quad \text{subject to} \quad \begin{pmatrix} A \\ A(T) \end{pmatrix} x = \begin{pmatrix} b_x \\ b_y \end{pmatrix}. \tag{4}$$

The key questions addressed in this paper are: How much can we gain from (4) relative to (1), under suitable assumptions from the viewpoint of compressed sensing? How can we cope with the unknown transformation T and recover it at the same time? Since T is usually a transformation of x between two subsequent points in time, we call (4) the *compressed motion sensing (CMS)* problem.

To approach this problem, we consider as a first step the following specific variant of (4): The vector x results from a discretization of a continuous medium observed on a grid graph, that covers a bounded Euclidean domain $\Omega \subset \mathbb{R}^{\dim}$, $\dim \in \{2, 3\}$. A concrete example is the setup of [7] related to the imaging in experimental fluid dynamics, where every component $x_i \in \{0, 1\}$, $i \in [n]$ indicates the absence or presence of a particle in a turbulent fluid. We adopt this scenario which is sufficient for our purpose to introduce the CMS problem.

Assuming a sufficiently fine spacing of the vertices i of the grid graph, any transformation $T\colon \Omega \to \Omega$ can be approximated by a permutation

$$y = Px, \qquad x \in \{0, 1\}^n, \tag{5}$$

which represents the motion of particles on the grid graph. As a consequence, the specific version of the *CMS sensor* of (4), that we study in this paper, reads

$$B := \begin{pmatrix} A \\ AP \end{pmatrix} \in \mathbb{R}^{2m\times n}. \qquad \text{(CMS sensor)} \tag{6}$$

Specifically, we are concerned with the following **objectives** of showing that:

1. the CMS sensor (6) effectively doubles the number of measurements and turns a poor sensor into a stronger one;
2. the vector $x \in \{0, 1\}^n$ can be recovered uniquely;
3. the transformation (5) in terms of the permutation matrix P can be *jointly* determined as well, together with x, by linear programming.

Points (1)–(3) are illustrated in Fig. 1 where $\Omega \subset \mathbb{R}^2$ is a square domain, uniformly tesselated by square pixels, and the sensor matrix A encodes sums of pixel values along all image rows and columns – cf. Fig. 2 and Eq. (7), also called projections. This simple setup of orthogonal projections is a classical scenario of

discrete tomography [4] and severely ill-posed. As Fig. 1 illustrates, however, our results show that even on the basis of such a poor sensor matrix A, the corresponding CMS sensor (5) enables to infer unique recovery and correspondence (motion) information (5) within a certain sparsity regime. In other words, *our approach turns a poor sensor into a stronger one*, while using overall the *same number* of $2m$ measurements.

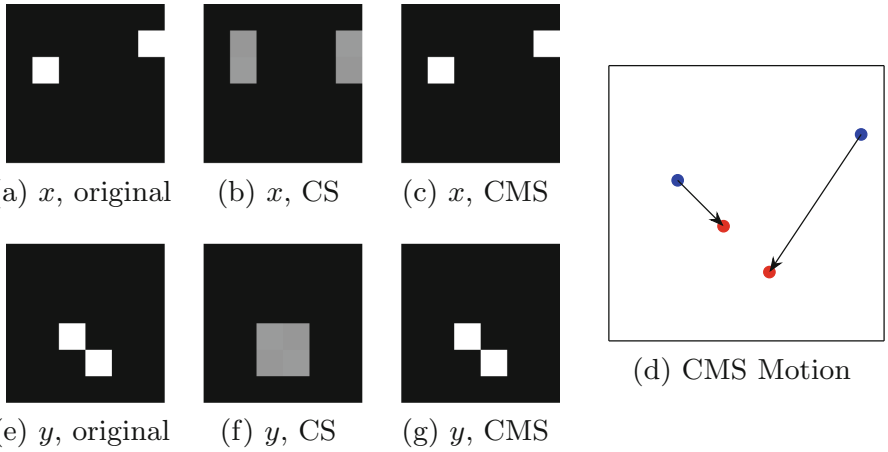

Fig. 1. Recovery of two sparse subsequent 6×6 vectors x (a) and y (e) by standard CS recovery via (1) and by compressed motion sensing (CMS), respectively, based on a sensor matrix A with projects along two orthogonal directions (rows and columns). Standard CS recovery (b, f) by solving (1) fails due to poor sensor properties of A, despite low sparsity. Using the same number of measurements the CMS sensor (6) leads to unique recovery (c, g) and correspondence (motion) information (d) so that $y = Px$.

Related Work. Our work builds on [7] where the connection between tomographic particle imaging and compressed sensing was established, along with an average case analysis of recovery conditions for *static* scenarios. In this paper, we establish the extension to more realistic *dynamic* scenarios. Applications include, in particular, the two-frame analysis of tomographic particle image sequences in experimental fluid dynamics (cf. Fig. 5).

Related other work includes [8] on the application of compressed sensing techniques to scene reconstruction in computer vision from multiple perspective views. The transformations are naturally restricted to low-dimensional Euclidean and affine transforms, and the recovery problem amounts to alternatingly minimizing a *non-convex* objective function. Our approach can deal with a significantly larger class of transformations and solve the *joint* problem of reconstruction and transformation estimation *globally optimal* by linear programming.

Our 'discretize-then-optimize' strategy adopted in this paper relates our recovery problem to *discrete optimal transport* [12]. The authors of [2] study *regularized* discrete optimal transport in connection with color transfer between natural images, where regularization enforces *spatially smooth* displacements. In this paper, we establish uniqueness of both recovery and displacements between particles solely based on a large subclass of one-to-one grid transformations, that includes also *non-smooth* displacement fields encountered in various applications.

A *continuous* variational approach based on optimal transport to object recovery from multiple tomographic measurements is studied in [1]. The numerical implementation of the approach seems to suffer from severe issues of numerical sensitivity and stability, and has only be applied to solid bodies of simple shapes. Related very interesting work, with a focus on dynamic tomography in experimental fluid dynamics, was published recently [9,10]. The authors adopt too a continuous PDE-based approach (iteratively linearized Monge-Ampère equation) which may lead to a more economical problem parametrization and enables, in particular, to take into account physical fluid flow models. On the other hand, a performance analysis is only provided for simple 1D settings or a single particle in 2D, and additional rectifying filters are needed if the approach is not discretized on a sufficiently fine grid.

Outside the field of mathematics, highly engineered state-of-the-art approaches to particle matching and tomographic recovery in experimental fluid dynamics, that require parameter tuning and do not provide any recovery guarantees, include [5,6,11].

2 Sparse Recovery Guarantees

In this section, we address objectives 1 and 2 as discussed in Sect. 1 and analyze sparse recovery of the vector x by compressed motion sensing. We adopt the scenario of [7].

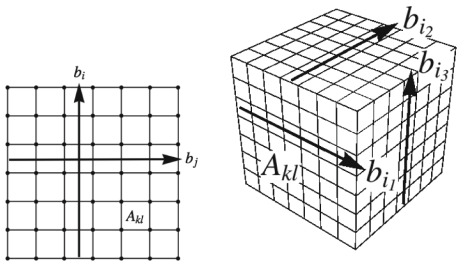

Fig. 2. LEFT: Imaging geometry with d^2 cells and $2d$ projection rays (here: $d = 6$) for problems of spatial dimension $D = 2$. RIGHT: Imaging geometry with d^3 cells and $3d^2$ rays (here: $d = 7$) for problems of spatial dimension $D = 3$. The corresponding sensor matrices A are given by (7).

We consider both dim = 2 and dim = 3 spatial dimensions. Figure 2 depicts the incidence geometry of the sensor A in terms of orthogonal projection rays The corresponding sensor matrices A are

$$A = \begin{pmatrix} \mathbb{1}_d^\top \otimes I_d \\ I_d \otimes \mathbb{1}_d^\top \end{pmatrix} \quad \text{if dim} = 2, \qquad A = \begin{pmatrix} \mathbb{1}_d^\top \otimes I_d \otimes I_d \\ I_d \otimes \mathbb{1}_d^\top \otimes I_d \\ I_d \otimes I_d \otimes \mathbb{1}_d^\top \end{pmatrix} \quad \text{if dim} = 3, \tag{7}$$

where the number d of pixels or voxels along each coordinate direction serves as discretization parameter.

We assume that

$$x \in \mathcal{X}_s^n := \left\{ z \in \{0,1\}^n \colon |\mathrm{supp}(z)| = s \right\} \tag{8}$$

is a uniformly drawn s-sparse vector and $P \in \Pi_n$ is a uniformly drawn permutation matrix. We next provide a *sufficient* condition in terms of sparsity s for unique recovery of $x \in \mathcal{X}_s^n$ via

$$\min_{z \in \mathbb{R}^n} \|z\|_1 \quad \text{subject to} \quad \begin{pmatrix} A \\ AP \end{pmatrix} z = \begin{pmatrix} Ax \\ APx \end{pmatrix}, \quad z \geq 0. \tag{9}$$

Since the columns of $B = \left(\begin{smallmatrix} A \\ AP \end{smallmatrix}\right)$ in (6) sum up to a constant the nonnegative constraints in (9) are self-regularizing.

Remark 1. Indeed, all elements z that satisfy $Bz = Bx$ have equal ℓ_1-norm

$$\|z\|_1 = \mathbb{1}_n^\top z = \frac{1}{2\,\mathrm{dim}} \mathbb{1}_{2m}^\top Bz = \frac{1}{2\mathrm{dim}} \mathbb{1}_{2m}^\top Bx = const.$$

Thus, in our setting, enforcing sparsity by ℓ_1-regularization (4) would be redundant. For sparse recovery we just need to take nonnegativity into account.

We next provide an average case analysis that guarantees unique recovery of a uniformly distributed random vector $x \in \mathcal{X}_s^n$ as the unique *nonnegative* of $Bz = Bx$. We closely follow [7] wherein the provided guarantees rest upon the following observation: A sparse vector $x \in \mathcal{X}_s^n$ will lead to a sparse measurement vector $b := Ax$. The support of b, denoted by

$$I_s := \mathrm{supp}(b) = \mathrm{supp}(Ax), \qquad x \in \mathcal{X}_s^n \tag{10}$$

is a random variable due to uniformly drawn random vectors x and the incidence geometry encoded by A. We denote its expected value by

$$m_s := \mathbb{E}\big[|I_s|\big] \leq m. \tag{11}$$

After removing the $m - |I_s|$ redundant rows from A, corresponding to zero-components of b, we may also remove every column corresponding to cells (pixels, voxels) that are met by any ray corresponding to a removed row. We denote the index set of the remaining columns by

$$J_s := [n] \setminus \{ j \in [n] \colon A_{ij} > 0,\ \forall i \in [m] \setminus I_s \}. \tag{12}$$

The resulting "effective" number $|J_s|$ of columns is a random variable with expected value denoted by

$$n_s := \mathbb{E}\big[|J_s|\big]. \tag{13}$$

For highly sparse scenarios with a very small sparsity s, every non-zero component of x creates multiple non-zero entries in b, because every cell (pixel, voxel)

intersects with multiple projection rays. As a consequence, the ratio $\frac{m_s}{n_s}$ is larger than 1. This ratio decreases with increasing s and in particular defines a critical maximal value

$$s_{\text{crit}} := \min\big\{s \in [n] \colon m_s/n_s \geq 1\big\}. \tag{14}$$

In [7], the authors computed the expected values m_s and n_s which enables to solve numerically (14) for s_{crit}. In addition, concentration inequalities were established that bound deviations of $|I_s|, |J_s|$ from their expected values m_s, n_s. In this work, we confine ourselves to computing m_s and n_s for the compressed motion sensor (6) and apply the previous considerations to the system $Bx = b$, with $b := Bx$ and $x \in \mathcal{X}_s^n$.

Lemma 1. *Let $X \in \mathcal{X}_s^n$ and $\mathcal{P} \in \Pi_n$ be independent and uniformly distributed random variables of s-sparse vectors $x \in \mathcal{X}_s^n$ and permutation matrices $P \in \Pi^n$. Then $Y = \mathcal{P}X \in \mathcal{X}_s^n$ is also uniformly distributed.*

Proof. Let $x, y \in \mathcal{X}_s^n$ be any realizations. Then there are $s!(n-s)!$ permutations P mapping x_S to y_S: $y = Px$. Denote this set by $\Pi^n(x; y)$ and count combinations of its elements with possible x from $\mathcal{X}_s^n$. □

Proposition 1. *Let the effective number of rows and columns of the sensor matrix (6) be indexed by*

$$I_s := \mathit{supp}(Bx), \quad x \in \mathcal{X}_s^n \qquad |I_s| \in [2m], \tag{15a}$$

$$J_s := [n] \setminus \{j \in [n] \colon B_{ij} > 0, \forall i \in [2m] \setminus I_s\}, \qquad |J_s| \in [n]. \tag{15b}$$

Assume the s-sparse vector $x \in \mathcal{X}_s^n$ is uniformly drawn. Then

$$m_s = \mathbb{E}\big[|I_s|\big] = 2\text{dim} \cdot d^{\text{dim}-1}\left(1 - \left(1 - \frac{1}{d^{\text{dim}-1}}\right)^s\right), \tag{16a}$$

$$n_s = \mathbb{E}\big[|J_s|\big] = d^{\text{dim}}\left(1 + \sum_{k=1}^{2\text{dim}} (-1)^k \binom{2\text{dim}}{k} \left(1 - \frac{k(d-1)+1}{d^{\text{dim}}}\right)^s\right). \tag{16b}$$

Proof. The proof basically generalizes the reasoning of [7, Lemma 5.1, Proposition 5.3] to the CMS matrix (6). Due to lack of space, we skip the details. □

As a result, the reconstruction of a random s-sparse nonnegative vector x will be based on a reduced linear system restricted to the rows I_s and the columns J_s. Dimensions of reduced systems will be the same for most random sets $S = \text{supp}(x) \subset J_s$ with $|S| = s$. Consequently, a sufficient condition that guarantees unique recovery of $x \in \mathcal{X}_s$ via

$$\text{find} \quad z \geq 0 \quad \text{subject to} \quad Bz = Bx, \tag{17}$$

is that the coefficient matrices B_{I_s, J_s} of the reduced systems are of full rank and overdetermined. B_{I_s, J_s} is on average overdetermined if the sparsity s is chosen according to (14), where s_{crit} solves

$$m_s = n_s, \tag{18}$$

with m_s, n_s defined in (16a) and (16b). Solving (18) for s_{crit} results in a curve that depends on the problem size d only, and is illustrated in Fig. 3a. To determine this curve we used a standard numerical root finding algorithm in order to compute the corresponding solution of (18) for each d in the plotted range.

Concerning the second issue, the full rank of B_{I_s,J_s}, we can resort to small random perturbations of the non-zero entries of A in (7), and thus preserving the sparse structure that encodes the underlying incidence relation of the sensor B. As a consequence the dimension of the reduced systems of a perturbed system does not change.

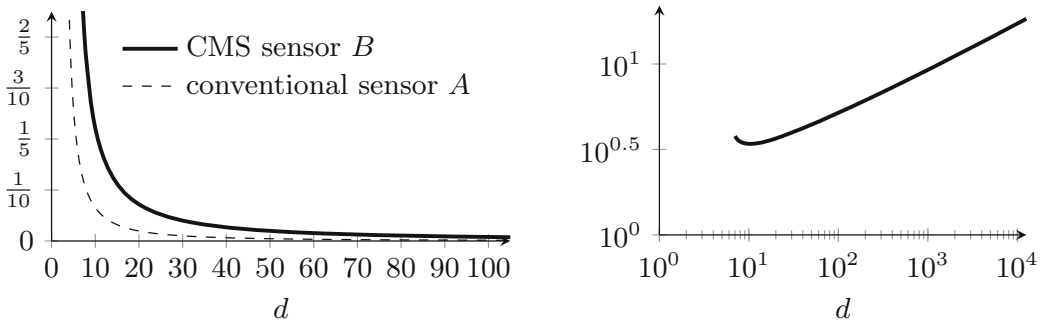

(a) Critical sparsities $\frac{s_{\text{crit}}}{n}$ (b) CMS sparsity performance gain

Fig. 3. Critical sparsity values $\frac{s_{\text{crit}}}{n}$ that enable with high probability unique recovery of s-sparse nonnegative vectors whenever $s \leq s_{\text{crit}}$, using sensor (7) for dim = 3 and the corresponding CMS sensor B in (a). Plot (b) shows the factor $\frac{s^A_{\text{crit}}}{s_{\text{crit}}}$ between the two functions in (a), that is the **theoretical sparsity performance gain of CMS**. This curve reaches a minimum of 3.4 and becomes larger than 17 for $d \geq 10^4$

The perturbed matrix $\tilde{A}$ is computed by uniformly perturbing the non-zero entries $A_{ij} > 0$ to obtain $\tilde{A}_{ij} \in [A_{ij} - \varepsilon, A_{ij} + \varepsilon]$, and by normalizing subsequently all column vectors of $\tilde{A}$ such that they all sum up to a constant e.g. equal to dim. We then define the "perturbed" CMS sensor as the CMS sensor (6) corresponding to $\tilde{A}$, i.e.

$$\tilde{B} := \begin{pmatrix} \tilde{A} \\ \tilde{A}P \end{pmatrix} \in \mathbb{R}^{2m \times n}. \tag{19}$$

We next give a sufficient condition that guarantees uniqueness of a nonnegative and sparse enough vector sampled by a CMS sensor of the form (19).

Proposition 2. *There exists a perturbed matrix $\tilde{A}$ that has the same structure as A from (7) such that the perturbed system $\tilde{B}z = \tilde{B}x$, with $\tilde{B}$ defined as in (19), admits unique recovery of s-sparse nonnegative vectors $x \in \mathcal{X}_s$ with high probability, i.e. the set*

$$\{z \in \mathbb{R}^n \colon \tilde{B}z = \tilde{B}x, z \geq 0\} \tag{20}$$

is a singleton with high probability, if s satisfies condition $s \leq s_{crit}$, where s_{crit} solves (18).

Proof. Analogously to [7, Proposition 5.10].

3 Joint Reconstruction and Motion Estimation

Displacement Estimation. We consider first the problem of determining the displacement mapping $P \in \Pi^n(x;y)$ from a *known* $x \in \mathcal{X}_s^n$ to a *known* $y \in \mathcal{X}_s^n$ (the joint problem is addressed below). Recall the particle imaging setup illustrated in Fig. 2: Every component $x_i, y_i \in \{0,1\}, i \in [n]$ indicates the absence or presence of a particle in a cell. We assume that the n cells have an arbitrarily fixed order and define the two support sets

$$S_x := \operatorname{supp}(x), \quad S_y := \operatorname{supp}(y). \tag{21}$$

The displacement corresponds to s moving particles and becomes an one-to-one *assignment* between the s cells in S_x and S_y. We associate with the assignment of $j \in S_x$ to $i \in S_y$ the cost C_{ij}. Then the *linear assignment* problem reads

$$\min_{P \in \mathcal{P}^n} \operatorname{tr}(C^\top P) \quad \text{subject to} \quad Px = y, P^\top x = y, P \geq 0, \tag{22}$$

where $\mathcal{P}^n := \{P \in \mathbb{R}_+^{n \times n} \colon P\mathbb{1} = \mathbb{1}, P^\top \mathbb{1} = \mathbb{1}\}$ is the Birkhoff polytop. This linear program is also a special case of the Kantorovich formulation of the *discrete optimal transport* problem [12]. $C \in \mathbb{R}_+^{n \times n}$ is the cost matrix related to the "energy" needed to move particles in x to y. It can be chosen based on physical prior knowledge about the scenario at hand – see Sect. 4.

Solving the Joint Problem. We now address the problem of *jointly* estimating x, y and the displacement between x and y in terms of $P \in \Pi^n(x;y)$ restricted to the supports (21). We define the assignment matrix $D \in \{0,1\}^{n \times n}$ as

$$D_{S_y, S_x} := P_{S_y, S_x} \in \Pi_s \quad \text{and} \quad D_{S_y^c, S_x^c} := 0. \tag{23}$$

Our approach is based on merging the CMS problem (4) with the linear assignment problem (22) into a single optimization problem, which reads

$$\begin{aligned} \min_{x,y,P} \operatorname{tr}\left(C^\top P\right) \quad \text{subject to} \quad & Ax = b_x, Ay = b_y, x, y \geq 0, \\ & Px = y, P^\top y = x, P \geq 0. \end{aligned} \tag{24}$$

Note that problem (24) is *block biconvex*: for each fixed (x,y) problem (24) is convex w.r.t. P, and it is also convex w.r.t. (x,y) for any fixed P. Rather than considering a block coordinate descent approach that sequentially updates the two blocks of variables (x,y) and P via proximal minimization, see e.g. [13], we replace the non-convex constraints $Px = y$, $P^\top y = x$ and solve instead the *linear program*

$$\begin{aligned} \min_{x,y,D} \operatorname{tr}\left(C^\top D\right) \quad \text{subject to} \quad & Ax = b_x, Ay = b_y, x, y \geq 0, \\ & D\mathbb{1} = y, D^\top \mathbb{1} = x, D \geq 0. \end{aligned} \tag{25}$$

Proposition 3. *Assume that $x, y \in \mathcal{X}_s^n$ and $P \in \Pi^n(x; y)$. Set $S_x = supp(x)$, $S_y = supp(y)$. Consider D from (23). If (x, y, D) is a solution of (24), then (x, y, D) is also a solution of (25). Likewise, a solution (x, y, D) of (25) is also a solution of (24).*

Proof. We have $Dx = D_{S_x} x_{S_x} = D\mathbb{1} = y$, $D^\top y = D_{S_y}^\top y_{S_y} = D^\top \mathbb{1} = x$ and hence (x, y, D) is feasible for both (24) and (25). □

Hence, the optimal assignment D between $x, y \in \mathcal{X}_s^n$ is a sparse matrix with s nonzero entries, that equals a permutation matrix when restricted to the support of x and y.

Corollary 1. *Consider $x \in \mathcal{X}_s$ that is mapped to $y = Px$ via $P \in \Pi_n(x; y)$. Then there exists a perturbation $\tilde{A}$ of A from (7) and a cost matrix $C \in \mathbb{R}_+^{n \times n}$ such that we can exactly recover x and y and the assignment matrix $D \in \{0, 1\}^{n \times n}$ from (23) with $y = Dx$ and $D_{S_y, S_x} := P_{S_y, S_x} \in \Pi_s$ with high probability by solving problem (25), specialized to*

$$\min_{u,v,D} tr\left(C^\top D\right) \quad \text{subject to} \quad \begin{array}{l} \tilde{A}u = \tilde{A}x, \tilde{A}v = \tilde{A}y, u, v \geq 0, \\ D\mathbb{1} = y, D^\top \mathbb{1} = x, D \geq 0, \end{array} \tag{26}$$

provided that $s \leq s_{crit}$, with s_{crit} solving (18).

Proof. By Proposition 2 there exists $\tilde{A}$ such that $x \in \mathcal{X}_s$ is the unique nonnegative solution of

$$\tilde{B}u = \begin{pmatrix} \tilde{A} \\ \tilde{A}P \end{pmatrix} u = \begin{pmatrix} \tilde{A} \\ \tilde{A}P \end{pmatrix} x = \begin{pmatrix} \tilde{A}x \\ \tilde{A}y \end{pmatrix}. \tag{27}$$

By Proposition 3 (x, y, D) with $D_{S_y, S_x} = P_{S_y, S_x} \in \Pi_s$ and $D_{S_y^c, S_x^c} := 0$ is a (vertex) solution of (26) for an appropriate $C \in \mathbb{R}_+^{n \times n}$.

The next section shows that in practice a perturbation of A is not necessary.

4 Experiments

In this section we empirically validate the previous theoretical results and illustrate the performance of the CMS approach in practice. We are concerned with the following issues:

(1) the exact recovery of sparse vectors $x \in \mathcal{X}_s$ by linear programming (17) when the CMS sensor B combines a poor tomographic sensor A (7) with a random permutation;
(2) the assignment matrix D from (23) in terms of the permutation matrix $P \in \Pi_n(x; y)$ can be jointly determined as well, together with x and y, by linear programming (25).

Exact Recovery of Sparse Vectors. We assess the sufficient sparsity s_{crit} (14) derived via Proposition 1 that induces overdetermined reduced systems and guarantees unique nonnegative recovery via a *perturbation* of CMS, see Proposition 2. Here we consider a CMS sensor B (6) that incorporates the *unperturbed* tomographic sensor A (7). Numerical experiments show that no perturbation of A is necessary in practice. We consider the particle recovery problem in three dimensions (dim = 3). For a fixed d, we vary the sparsity s in order to determine empirically the *critical* sparsity that guarantees unique recovery of s-sparse vectors sampled by B via (17). For each d and s, we generate a permutation matrix P uniformly at random as part of the CMS sensor B and a random binary signal $x \in \mathcal{X}_s^n$ with uniform support. Form $b = Bx$ we recover $\hat{x}$ by solving the LP (17). If the recovery error $\|x - \hat{x}\|_2 < 10^{-8}$, we declare recovery successful. We repeat this experiment 200 times and count the success ratio, plotted in Fig. 4.

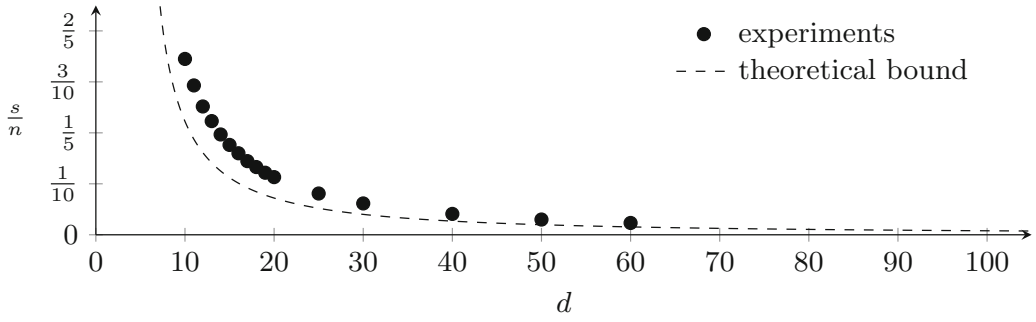

Fig. 4. Experimental validation of the derived recovery guarantee from Proposition 1 for dim = 3. The empirical relative sparsity $\frac{s}{n}$ (black dots) that separates recovery from nonrecovery together with the *sufficient* theoretical sparsity bound s_{crit} (14) for comparison. We note that perturbation of A in view of Proposition 2 was not necessary, but critical when using only the static sensor A according to [7].

Joint Recovery and Motion Estimation. The minimal example shown in Fig. 1 already illustrates the potential of CMS. More realistic scenarios are shown in Fig. 5 using a cost matrix filled with Euclidean distances between grid nodes. The underlying motion was generated by discretizing a turbulent random vector field to grid positions in order to be captured by a permutation.

The critical role of the cost matrix via (25) is illustrated in Fig. 6. We generate a vector field $y \in \mathbb{R}^3$ from $x \in \mathbb{R}^3$ by

$$y = \begin{pmatrix} \cos(\alpha) & \sin(\alpha) & 0 \\ -\sin(\alpha) & \cos(\alpha) & 0 \\ 0 & 0 & 1 \end{pmatrix} x + \begin{pmatrix} 0 \\ 0 \\ v_z \end{pmatrix} \tag{28}$$

with $\alpha = \text{rad}(5v_z)$. This represents a rotation around and a constant shift along the z-axis. $v_z \in \mathbb{N}$ is the vertical velocity on a voxel basis. In addition to an Euclidean cost matrix, we define a cost matrix that penalizes particles that do not move along their orbit around the z-axis, i.e.

$$C_{i,j} = \min_z \left\{ \|z - w_j\|_2^2 \ : \ \left\| \begin{pmatrix} z_1 \\ z_2 \end{pmatrix} \right\| = \left\| \begin{pmatrix} w_{i,1} \\ w_{i,2} \end{pmatrix} \right\| \right\} \tag{29}$$

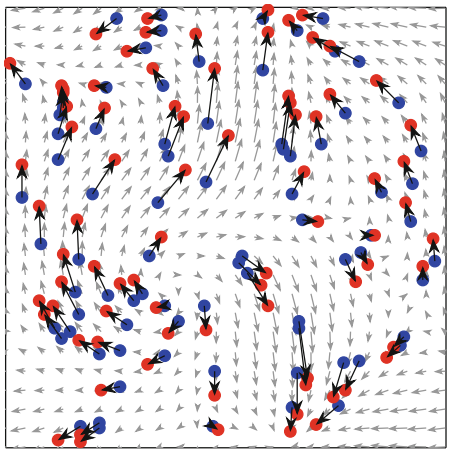

(a) CMS recovery of 80 particles on a 256×256 grid.

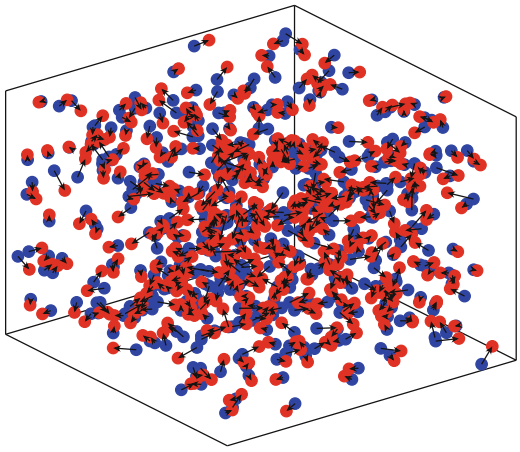

(b) CMS recovery of 500 particles on a $256 \times 256 \times 256$ grid.

Fig. 5. Exact CMS recovery of particles (blue and red dots) and the assignment (black arrows) via (25). The true motion is shown as gray arrows. (a) Sensor A from (7) is complemented with two more projections at 45 and 135° to define CMS. In (b) the 3 projection sensor A from (7) is used. (Color figure online)

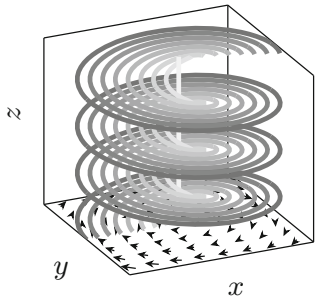

(a) underlying motion

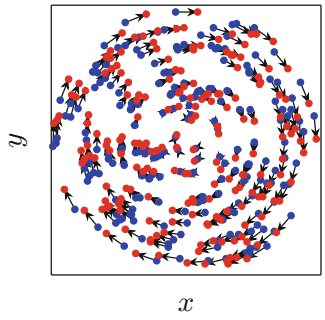

(c) $v_z = 2$, $\alpha = 10$, Eucl. C

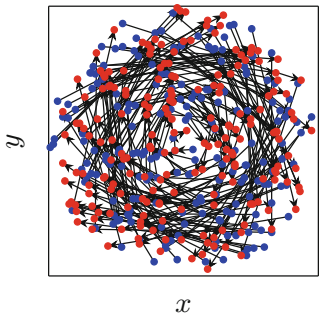

(e) $v_z = 18$, $\alpha = 90$, Orb. C

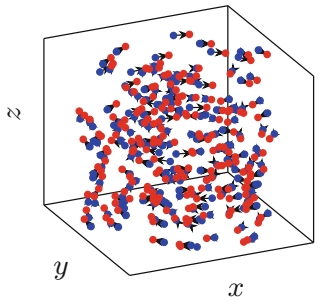

(b) $v_z = 2$, $\alpha = 10$, Eucl. C

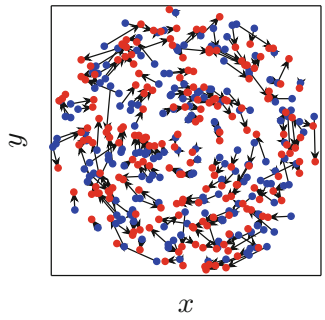

(d) $v_z = 4$, $\alpha = 20$, Eucl. C

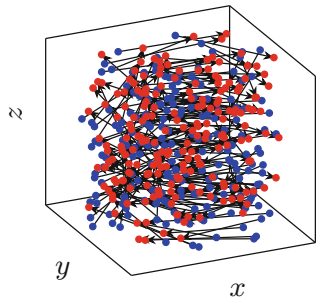

(f) $v_z = 18$, $\alpha = 90$, Orb. C

Fig. 6. Vortex motion (28) in a $257 \times 257 \times 257$ volume with additional vertical shift v_z (a) and recovered assignments by CMS (b)–(f). Recovery of particles and assignment is exact when the cost matrix C is Euclidean, if displacements are small, i.e. $v_z = 2$ and $\alpha = 10$ (b), (c). After increasing both, recovery with an Euclidean C fails (d), but CMS is still capable of recovering the correct motion by using a different cost matrix (29) called *Orbit* C here. Even for comparably large displacements the CMS recovery is perfect (e), (f).

with voxel locations $w_i \in \mathbb{Z}^3$. The result for 200 moving particles according to (28) and different values of velocity v_z are shown in Fig. 6. Using (29) perfect motion recovery is possible even for large displacements. This shows the flexibility of our framework in incorporating motion priors.

5 Conclusion

We introduced "Compressed Motion Sensing", a novel framework the exploits sparsity for recovery within dynamic scenarios. We gave theoretical recovery guarantees and validated them experimentally. The approach can be flexibly adapted to a broad range of applications that involve physical prior knowledge. Besides signal reconstruction, motion is recovered too, by using in a cost-effective way undersampled measurements of a single sensor at multiple points in time.

References

1. Abraham, I., Abraham, R., Bergounioux, M., Carlier, G.: Tomographic reconstruction from a few views: a multi-marginal optimal transport approach. Appl. Math. Optim. **75**(1), 55–73 (2017)
2. Ferradans, S., Papadakis, N., Peyré, G., Aujol, J.: Regularized discrete optimal transport. SIAM J. Imaging Sci. **7**(3), 1853–1882 (2014)
3. Foucart, S., Rauhut, H.: A Mathematical Introduction to Compressive Sensing. Springer, Heidelberg (2013)
4. Herman, G.T., Kuba, A.: Discrete Tomography: Foundations Algorithms and Applications. Birkhäuser, Basel (1999)
5. Lynch, K.P., Scarano, F.: An efficient and accurate approach to MTE-MART for time-resolved tomographic PIV. Exp. Fluids **56**(3), 1–16 (2015)
6. Novara, M., Batenburg, K.J., Scarano, F.: Motion tracking-enhanced MART for tomographic PIV. Meas. Sci. Technol. **21**(3), 035401 (2010)
7. Petra, S., Schnörr, C.: Average case recovery analysis of tomographic compressive sensing. Linear Algebra Appl. **441**, 168–198 (2014)
8. Puy, G., Vandergheynst, P.: Robust image reconstruction from multiview measurements. SIAM J. Imaging Sci. **7**(1), 128–156 (2014)
9. Saumier, L., Khouider, B., Agueh, M.: Optimal transport for particle image velocimetry. Commun. Math. Sci. **13**(1), 269–296 (2015)
10. Saumier, L., Khouider, B., Agueh, M.: Optimal transport for particle image velocimetry: real data and postprocessing algorithms. SIAM J. Appl. Math. **75**(6), 2495–2514 (2015)
11. Schanz, D., Gesemann, S., Schröder, A.: Shake-the-box: lagrangian particle tracking at high particle image densities. Exp. Fluids **57**(70), 1–27 (2016)
12. Villani, C.: Optimal Transport: Old and New. Grundlehren der mathematischen Wissenschaften. Springer, Heidelberg (2009)
13. Xu, Y., Yin, W.: A block coordinate descent method for regularized multiconvex optimization with applications to nonnegative tensor factorization and completion. SIAM J. Imaging Sci. **6**(3), 1758–1789 (2013)